Available online at ScienceDirect

Nuclear Engineering and Technology

journal homepage: www.elsevier.com/locate/net

Original Article

Effect of Oxidation on the Fatigue Crack Propagation Behavior of Z3CN20.09M Duplex Stainless Steel in High Temperature Water

Huan Chun Wu [a,b], *Bin Yang* [a,c,*], *Yue Feng Chen* [c], *and Xu Dong Chen* [c]

[a] *State Key Laboratory for Advanced Metals and Materials, University of Science and Technology Beijing, 30 XueYuan Road, Beijing 100083, China*

[b] *Life Assessment Center, Suzhou Nuclear Power Research Institute, 1788 XiHuan Road, Suzhou 215004, China*

[c] *Collaborative Innovation Center of Steel Technology, Beijing 100083, China*

ARTICLE INFO

Article history:
Received 9 June 2016
Received in revised form
4 December 2016
Accepted 25 December 2016
Available online 30 January 2017

Keywords:
Corrosion Fatigue
Duplex Stainless Steel
Fatigue Crack Propagation
Oxide Film
X-ray Photoelectron Spectroscopy

ABSTRACT

The fatigue crack propagation behaviors of Z3CN20.09M duplex stainless steel (DSS) were investigated by studying oxide films of specimens tested in 290°C water and air. The results indicate that a full oxide film that consisted of oxides and hydroxides was formed in 290°C water. By contrast, only a half-baked oxide film consisting of oxides was formed in 290°C air. Both environments are able to deteriorate the elastic modulus and hardness of the oxide films, especially the 290°C water. The fatigue lives of the specimens tested in 290°C air were about twice of those tested in 290°C water at all strain amplitudes. Moreover, the crack propagation rates of the specimen tested in 290°C water were confirmed to be faster than those tested in 290°C air, which was thought to be due to the deteriorative strength of the oxide films induced by the mutual promotion of oxidation and crack propagation at the crack tip. It is noteworthy that the crack propagation can be postponed by the ferrite phase in the DSS, especially when the specimens were tested in 290°C water.

1. Introduction

Duplex stainless steels (DSSs) consisting of ferrite (α) and austenite (γ) are extensively used in the chemical and oil industries, marine engineering and nuclear power plants. They often have outstanding mechanical and corrosion properties [1–9]. Among the DSSs, Z3CN20.09M DSS (MaNuEr Nuclear Power Equipment Company, YanTai, ShanDong Province, China) has been widely used to produce the primary coolant pipes of pressured water reactor nuclear power plants. It is well known that the temperature and pressure of water in the component often fluctuate during operation, which can subject the pipes to cyclic thermal stresses. Meanwhile, the startup and shutdown processes of a nuclear power plant can also induce similar results [10]. Consequently, the primary coolant pipes are known to often suffer corrosion fatigue (CF) failure under the combination of cyclic stress and high temperature water environment during

* *Corresponding author.*
E-mail address: byang@ustb.edu.cn (B. Yang).
http://dx.doi.org/10.1016/j.net.2016.12.017

the service period [11–14]. However, because of the complexity of the CF process, only a few studies have been aimed at the CF behavior of stainless steels [15].

Undoubtedly, the fatigue crack propagation rate can be accelerated by a high temperature water environment. The effect of the environment on crack propagation is often attributed to the interaction of the environment and the crack tip during fatigue tests [12, 16–18]. It is well known that fresh metal on a crack tip can be oxidized or hydrogenated easily in high temperature water, which can induce hydrogen embrittlement or hydrogen assisted cracking [12, 16, 17]. Meanwhile, the metal atoms in the crack tip can be dissolved by high temperature water [16, 17, 19]. Both of these processes can accelerate crack propagation and decrease the fatigue life of stainless steels. However, all of the studies only speculated on the deterioration mechanism of the crack tip, without related evidence to verify that mechanism. To some extent, the effect of high temperature water environment on fatigue crack propagation can be regarded as an oxidation process at the crack tip. Thus, the composition and mechanical properties of an oxide film formed in a high temperature water environment should play an important role in the crack propagation behavior of stainless steels. In fact, a number of studies have focused on identifying the morphology, thickness, composition, and structure of oxide films formed on the surface of stainless steels in high temperature water [20–25]. However, very little work has been aimed at establishing a correlation between the oxidation and the fatigue crack propagation of stainless steels.

In this study, the fatigue crack propagation behaviors of Z3CN20.09M DSS in water and air at a temperature of 290°C were investigated. The composition, elastic modulus and hardness of the oxide films formed in both environments were identified. Based on the experimental results, the effect of oxidation on the fatigue crack propagation process was analyzed. Moreover, a postponing effect of the ferrite phase in Z3CN20.09M DSS on crack propagation was also elucidated.

2. Materials and methods

2.1. Material

The outer diameter and wall thickness of the pipe used for the tests were 935 mm and 65 mm, respectively. All specimens were cut from the middle of the cross section. The chemical composition of Z3CN20.09M DSS is shown in Table 1. The pipe was fabricated by first using electric-arc and argon–oxygen decarburization melting, and then by using casting and solution treatment at 1,180°C for 8 hours. The typical microstructure is an island-like ferrite (α) and austenite (γ) matrix. The volume fraction of the ferrite is about 15%, as shown in Fig. 1.

Table 1 – Chemical composition of Z3CN20.09M DSS (wt.%).

C	Si	Mn	P	S	Cr	Ni	Mo	N	Fe
0.024	1.09	1.11	0.023	0.039	20.16	9.06	0.26	0.033	Balance

DSS, duplex stainless steel.

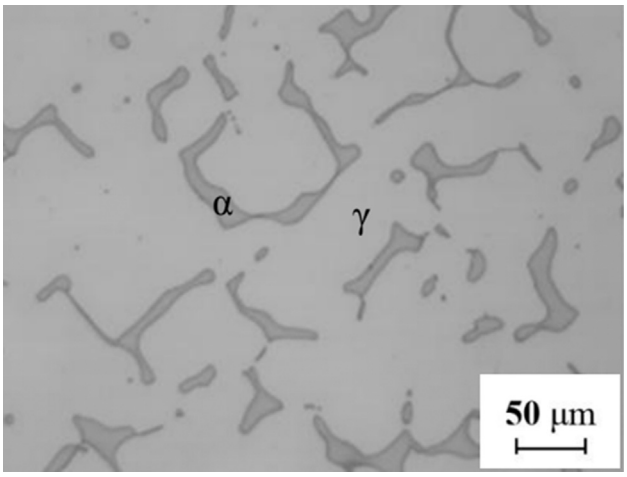

Fig. 1 – Microstructure of the Z3CN20.09M DSS. DSS, duplex stainless steel.

2.2. CF test

According to the standard of ASTM (American Society for Testing of Materials) E606, cylindrical fatigue specimens with gauge length and diameter of 14 mm and 7 mm, respectively, were used for the CF test, as shown in Fig. 2. All fatigue tests were conducted on a CF cracking system (PO103, KNR Company, Gyeonggi-do, Republic of Korea) with a capacity dynamic load of 20 kN and an SS static autoclave. The instrument was operated by a computer-controlled servo electric system. All fatigue tests used the strain control mode. The strain was measured using a linear variable differential transformer extensometer. The solution used for the tests was distilled water. The fatigue test parameters and the water chemistry are shown in Table 2. Prior to the crack propagation tests, each specimen was given a precrack with a depth of 300 μm in the middle of the gauge. During the CF tests, the precrack depths were measured by sequentially interrupting after different cycles using optical microscopy. After the CF

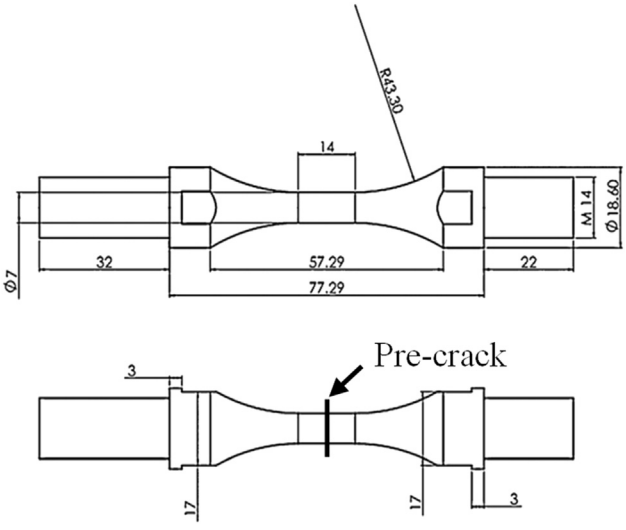

Fig. 2 – Schematic layout of the corrosion fatigue testing specimen (mm).

Table 2 – Test parameters and high temperature water chemistry.

Wave form	Strain amplitude	Strain rate	Temperature	Pressure	Dissolved oxygen	pH	Conductivity
Triangle	±0.5%, ±1.0%	0.1% s^{-1}	290°C	8 MPa	10 ppm (wt.%)	6.6	0.15 μS/cm

tests, fractures were observed by scanning electron microscopy (SEM; Zeiss Supra55; Carl Zeiss, Jena, Germany). All fatigue tests were carried out in 290°C water and air in same autoclave.

2.3. *Oxide film test*

As is well known, the fatigue fractures of specimens are too rough to be studied by X-ray photoelectron spectroscopy (XPS) and nanomechanical probe. Therefore, substitute specimens must be prepared. During the CF test, the fresh metal aroused at the crack tip was active and easy to oxidize. Thus, the oxygen content in the crack tip of the specimen was often nearly the same as that in the oxide film of the specimen tested for a longer time under the same environment. The energy-dispersive X-ray spectroscopy results shown in Table 3 indicate that the oxygen contents in the crack tips were approximately equal to those in the oxide films after testing for 72 hours under the same environment. So, the oxide films of the specimens oxidized for 72 hours can act as fractures. To compare the two kinds of oxide film, specimens were evaluated after they were heat treated at 290°C in a vacuum environment, which was also conducted using a nanomechanical probe. All tests were conducted using the continuous stiffness measurement (CSM) mode.

Table 3 – Oxygen contents in the fatigue fractures and films oxidized for 72 hours in 290°C water and air environments (at.%).

Specimen/ environment	Fracture		Oxide film	
	Water	Air	Water	Air
Oxygen content	40.19	5.92	40.01	6.14

3. Results and discussion

3.1. *Compositions and mechanical properties of oxide films*

Figs. 3A–3C show the detailed XPS spectra of Fe $2p_{3/2}$, Cr $2p_{3/2}$ and Ni $2p_{3/2}$ of the oxide films tested in 290°C water and air,

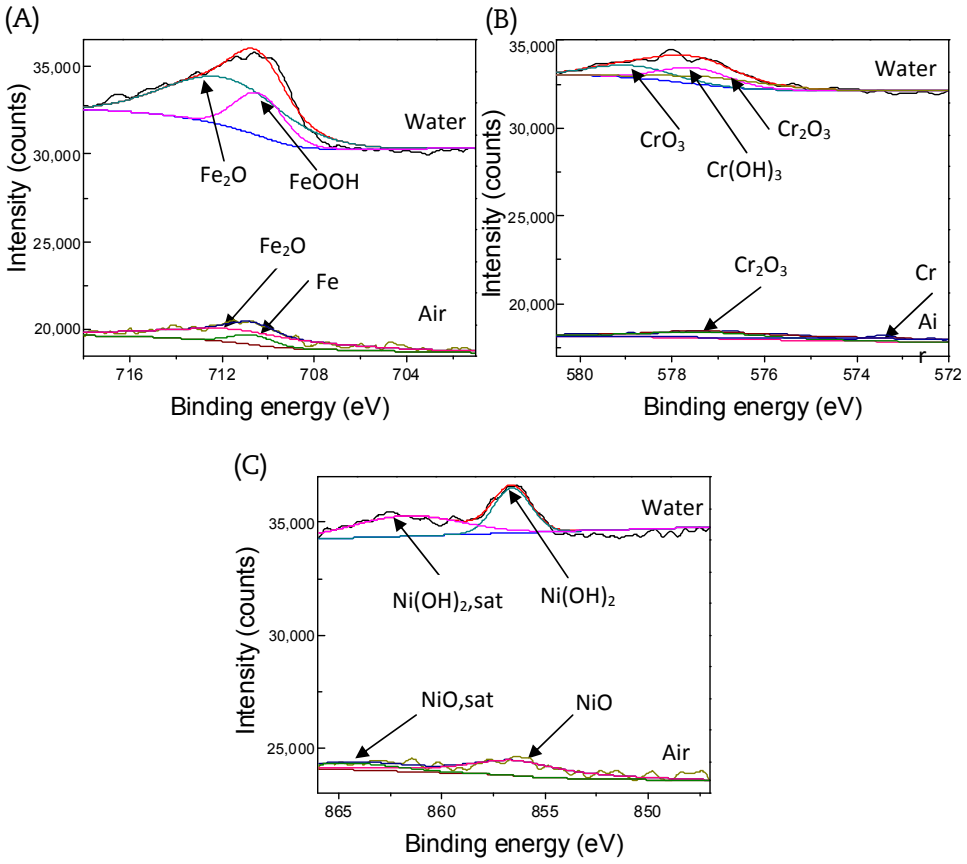

Fig. 3 – Detailed XPS spectra peaks collected from oxide films tested in 290°C water and air. (A) Fe 2p3/2. (B) Cr 2p3/2. (C) Ni 2p3/2. XPS, X-ray photoelectron spectroscopy.

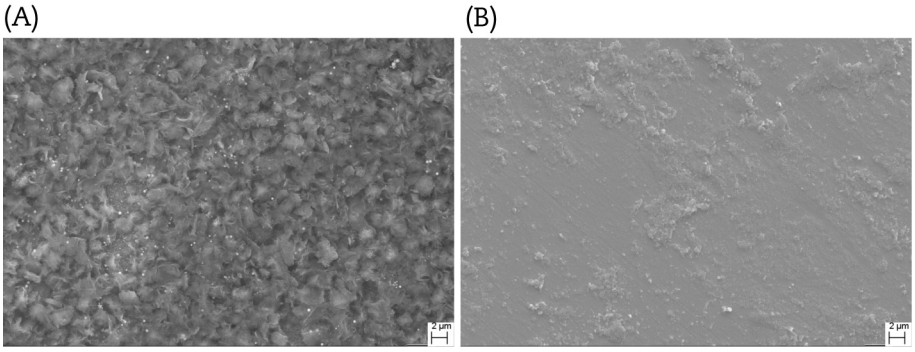

Fig. 4 – Oxide film morphologies of specimens tested for 72 hours in different environments. (A) 290°C water. (B) 290°C air.

respectively. The background subtraction was obtained by Shirley type [26,27]. All the main peaks were fitted by XPSPEAK4.1 software to obtain the subsidiary peaks. During the quantitative evaluation, all species were distinguished based on their binding energies shown in the *NIST X-ray Photoelectron Spectroscopy Handbook* [28]. From this figure, it can be seen that the intensities of the peaks for the specimens tested in 290°C water were much higher than those tested in 290°C air. In the 290°C water environment, the main peaks of Fe $2p_{3/2}$, Cr $2p_{3/2}$ and Ni $2p_{3/2}$ positioned at approximately 710.62 eV, 577.82 eV, and 856.34 eV, respectively, can likely be attributed to Fe_2O_3 and FeOOH, $Cr(OH)_3$, CrO_3 and Cr_2O_3, as well as $Ni(OH)_2$. In the 290°C air environment, the main peaks of Fe $2p_{3/2}$, Cr $2p_{3/2}$, and Ni $2p_{3/2}$ positioned at approximately 711.01 eV, 577.29 eV, and 856.51 eV, respectively, were likely attributable to Fe_2O_3 and metallic Fe, Cr_2O_3 and metallic Cr, as well as NiO [22]. These results are in agreement with those of previous studies [21,22,24,26].

In summary, a full oxide film consisting of oxides and hydroxides was formed in the 290°C water environment. By contrast, only a half-baked oxide film consisting of oxides was formed in the 290°C air environment. Fig. 4 shows the SEM morphologies of the oxide films tested under both environments. The figure indicates that Z3CN20.09M DSS was easier to oxidize in 290°C water than in 290°C air. The oxygen contents of the oxide films further verify this judgment, as shown in Table 3.

Fig. 5 shows the elastic modulus and hardness of the surface of the specimens after they were tested under 290°C vacuum, water, and air environments. Obviously, the specimen tested in 290°C vacuum had the highest values among all the specimens, showing that both 290°C water and air can deteriorate the elastic modulus and hardness of the oxide films, especially 290°C water. Fig. 4 also shows that a number of compound particles were distributed on the surface of the specimen tested in 290°C water, which destroyed the consecutiveness of the oxide films, whereas only a few particles were distributed on the surface of the specimen when tested in 290°C air. Meanwhile, the surface of the specimens can also be corroded by the high temperature water. Therefore, the elastic modulus and hardness of the oxide films tested in 290°C water were worse than those tested in 290°C air.

3.2. *Crack propagation of Z3CN20.09M DSS*

Fig. 6 shows the cyclic stress response curves of the Z3CN20.09M DSS specimens tested in 290°C water and air. One can see that the fatigue lives of the specimens tested in 290°C air were about twice those of specimens tested in 290°C water

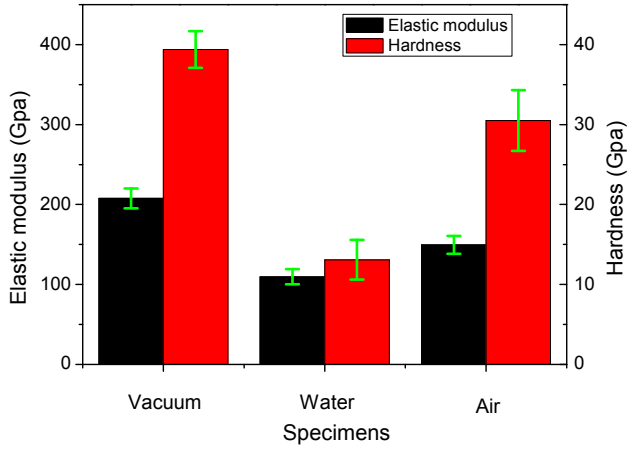

Fig. 5 – Elastic modulus and hardness of the specimen surface after tested in 290°C vacuum, water, and air environments for 72 hours.

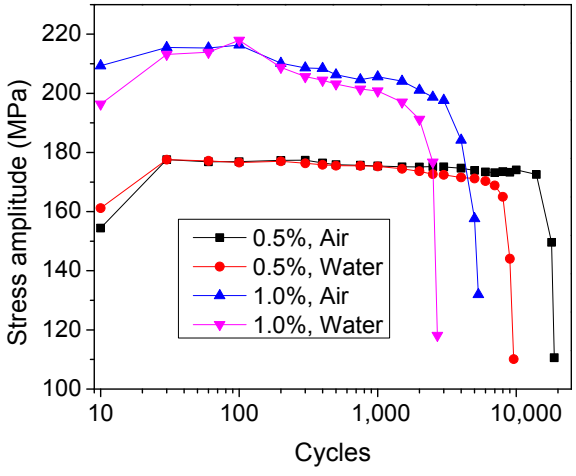

Fig. 6 – Cyclic stress response curves of the specimens tested in 290°C water and air at different strain amplitudes.

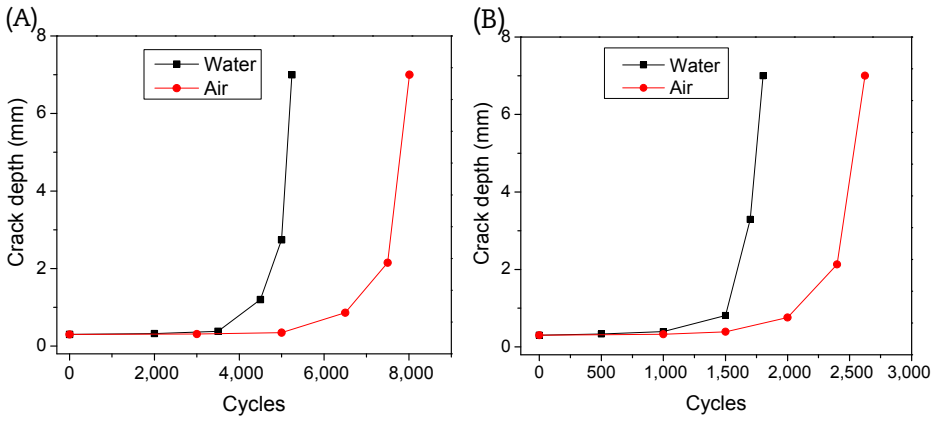

Fig. 7 – Crack depths as a function of fatigue cycles of the specimens tested in 290°C water and air at different stain amplitudes. (A) ±0.5%. (B) ±1.0%.

at all strain amplitudes. Fig. 7 shows the crack depths as a function of the fatigue cycles of the specimens tested in 290°C water and air at strain amplitudes of ±0.5% and ±1.0%, respectively. It can be seen that all cracks in 290°C water reached the limit depth earlier than those in 290°C air. Obviously, oxidation at the crack tips of the specimens tested in 290°C water can accelerate the fatigue crack propagation process.

During the fatigue test, the precrack propagation rate increased as the fatigue cycle continued. It can be divided into three stages, i.e., crack propagates at very slow rate, slow rate, and fast rate [29–31]. At the beginning of the first stage, the precrack tip was negative and the process of oxidation was slow. Fig. 8A shows the precrack morphology. After a long period of oxidation, the oxide film formed at the precrack tip and its strength deteriorated. Because of the lower strength of the oxide films formed in 290°C water, the precracks started to propagate earlier. In the second stage, the crack propagation rate increased. One can see obvious fatigue stripes on the fracture even though the separation between those stripes was narrow, indicating that the crack propagation rate was slow, as shown in Fig. 8B. In the third stage, the crack propagation rate was the fastest owing to the increase in crack depth and stress intensity. So the separation of the fatigue stripes in the fracture was wide, as shown in Fig. 8C. During all three stages, the oxidation was always promoted by crack propagation because of the fresh metal aroused at the crack tip, especially at the last stage. On the other hand, crack

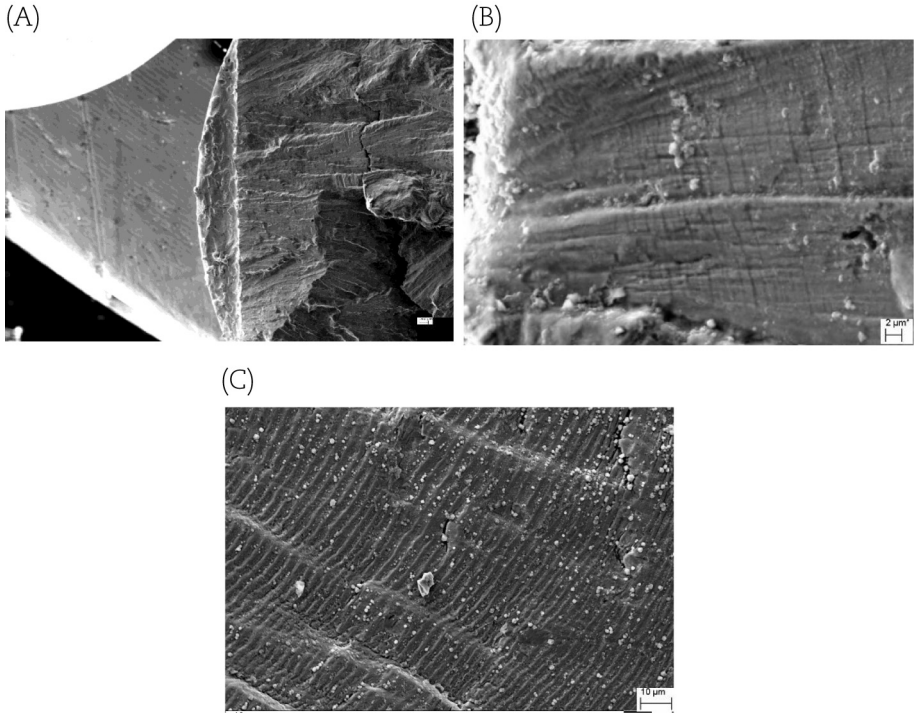

Fig. 8 – Fatigue stripes morphologies at the different crack propagation rates of the precracked specimen tested in 290°C water at strain amplitude of ±0.5%. (A) Precrack morphology. (B) At slow rate. (C) At fast rate.

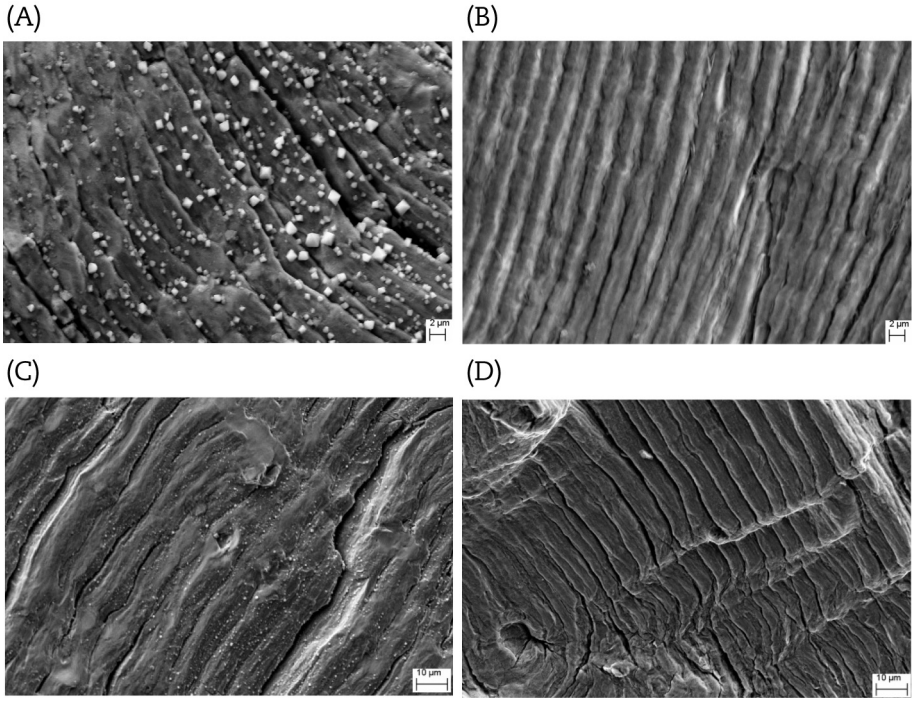

Fig. 9 – Fatigue stripe morphologies for the different environments and strain amplitudes at the third stage. (a) ±0.5% in 290°C water, (b) ±0.5% in 290°C air, (c) ±1.0% in 290°C water and (d) ±1.0% in 290°C air.

propagation was also promoted by oxidation, which induced a low strength of the oxide films at the crack tip. This means that crack propagation and oxidation can promote each other for the whole fatigue process of the precracked specimen [32]. Consequently, crack propagation for the specimens tested in 290°C water was faster owing to the more serious oxidation. Fig. 9 shows the fatigue stripe morphologies of the precracked specimens tested in different environments and strain amplitudes in the third stage. The average separations of the fatigue stripes for the four precracked specimens were approximately 3.7 μm, 1.9 μm, 12.6 μm, and 5.4 μm, respectively. They are in coincidence with the average crack propagation rates of the specimens in the third stage. In fact, the three stages mentioned above will occur in any general fatigue process, and can be accelerated by a detrimental environment such as high temperature water.

3.3. *Effect of ferrite phase on crack propagation rate*

According to previous studies [33,34], the corrosion resistances of ferrite and austenite phases in a DSS often depend on the pitting resistance equivalent numbers (PRENs). The pitting corrosion resistance is better for a higher PREN, which can be calculated as PREN = %Cr + 3.3%Mo + 20%N. The PRENs calculated for ferrite and austenite in the Z3CN20.09M DSS are shown in Table 4. Obviously, the ferrite phase has a better corrosion resistance.

Moreover, the austenite phase is softer than the ferrite phase because of its different crystal structure [35,36]. Thus, the austenite phase was more easily deformed than the ferrite phase, and persistent slip bands (PSBs) often formed in the austenite phase during the fatigue test. Undoubtedly, the PSBs can damage the crystal structure and deteriorate the corrosion resistance of the austenite phase [11,37,38]. Therefore, the austenite phase in the specimens should be preferentially corroded in 290°C water. Similarly, the deformed austenite in the crack tip can also be easily corroded by 290°C water during the CF test. Consequently, the ferrite phase in the specimens can postpone crack propagation because of the higher strength and relative better corrosion resistance. This process can be explained by using a model, as shown in Fig. 10.

During the CF test, short cracks were mainly initiated in the austenite phase, as shown in Fig. 10A. As the fatigue loading continued, PSBs were formed in the austenite phase, as shown in Fig. 10B. The deformed austenite phase at the crack tip was easily corroded by high temperature water. Then, the ferrite phase was aroused with the crack propagation, as shown in Fig. 10C. As mentioned previously, the ferrite phase has a relatively better corrosion resistance and higher strength than the austenite phase at the crack tip, so crack propagation can be postponed by the ferrite phase, as shown in Fig. 10D. Consequently, the island-like ferrite phase decreased the crack propagation rate and enhanced the fatigue life of the specimens when tested in 290°C water.

In fact, the ferrite phase can often retard fatigue crack propagation in an air environment of the DSS. Some

Table 4 – PREN values of ferrite and austenite phases of Z3CN20.09M DSS.

Phases	Cr	Mo	N	PREN
Ferrite	25.84	0.28	0.023	27.22
Austenite	19.71	0.23	0.037	21.21

DSS, duplex stainless steel; PREN, pitting resistance equivalent number.

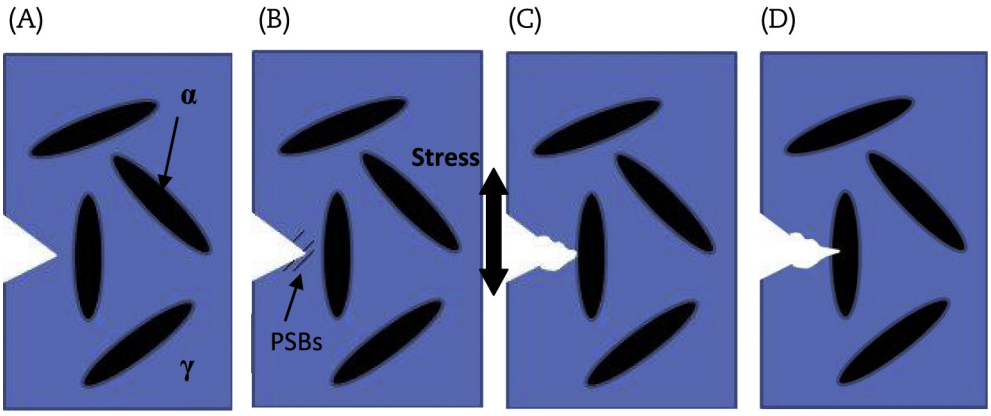

Fig. 10 – A model in which a crack propagation process is postponed by the ferrite phase at the crack tip of specimen tested in 290°C water. (A) One of fatigue cracks. (B) Persistent slip bands (PSBs) are formed in the austenite at the crack tip. (C) Deformed austenite is corroded by 290°C water. (D) Crack propagation is postponed by a ferrite phase.

researchers [3,39,40] have measured the crack length using *in situ* experiments, with results indicating that crack propagation often slows down for a certain period in the ferrite phase during fatigue testing of DSS. This has often been attributed to the effective barriers of the phase boundary and high strength of the ferrite phase. In the present study, the combined effect of the better corrosion resistance and the higher strength of the ferrite phase finally decreased the crack propagation rate.

4. Conclusion

(1) The oxidation of Z3CN20.09M DSS was more serious in 290°C water than in 290°C air. A full oxide film consisting of oxides and hydroxides was formed in 290°C water. By contrast, only a half-baked oxide film consisting of oxides was formed in 290°C air.
(2) There are more compound particles formed in oxide films tested in 290°C water than in oxide films tested in 290°C air, which decreases the elastic modulus and hardness of the oxide films, especially in 290°C water.
(3) The fatigue lives of specimens tested in 290°C air were about twice of those tested in 290°C water. The crack propagation rates of specimens tested in 290°C water were markedly faster than those of specimens tested in 290°C air.
(4) In 290°C water, the austenite phase of the Z3CN20.09M DSS was easily deformed with lower PREN and thus could be corroded more easily than the ferrite phase. The island-like ferrite phase can postpone fatigue crack propagation, especially when the specimens were tested in 290°C water.

Conflicts of interest

The authors declare no conflict of interest.

Acknowledgments

The authors gratefully acknowledge the financial support from the "863" Program of China under grant No. 2012AA03A507.

REFERENCES

[1] L. Llanes, A. Mateo, P. Villechaise, J. Méndez, M. Anglada, Effect of testing atmosphere (air/in vacuo) on low cycle fatigue characteristics of a duplex stainless steel, Int. J. Fatigue 21 (1999) S119–S125.
[2] Y.Q. Wang, J. Han, H.C. Wu, B. Yang, X.T. Wang, Effect of sigma phase precipitation on the mechanical and wear properties of Z3CN20.09M cast duplex stainless steel, Nucl. Eng. Des 259 (2013) 1–7.
[3] R. Strubbia, S. Hereñú, A. Giertler, I. Alvarez-Armas, U. Krupp, Experimental characterization of short crack nucleation and growth during cycling in lean duplex stainless steels, Int. J. Fatigue 65 (2014) 58–63.
[4] S. Li, Y. Wang, H. Zhang, S. Li, G. Wang, X. Wang, Effects of prior solution treatment on thermal aging behavior of duplex stainless steels, J. Nucl. Mater. 441 (2013) 337–342.
[5] S.L. Li, Y.L. Wang, H.L. Zhang, S.X. Li, K. Zheng, F. Xue, X.T. Wang, Microstructure evolution and impact fracture behaviors of Z3CN20-09M stainless steels after long-term thermal aging, J. Nucl. Mater. 433 (2013) 41–49.
[6] G. Chai, Fatigue behaviour of duplex stainless steels in the very high cycle regime, Int. J. Fatigue 28 (2006) 1611–1617.
[7] Y.Q. Wang, B. Yang, J. Han, H.C. Wu, X.T. Wang, Effect of precipitated phases on the pitting corrosion of Z3CN20.09M cast duplex stainless steel, Mater. Trans. 54 (2013) 839–843.
[8] J.K. Sahu, U. Krupp, R.N. Ghosh, H.J. Christ, Effect of 475°C embrittlement on the mechanical properties of duplex stainless steel, Mater. Sci. Eng. A 508 (2009) 1–14.
[9] J.K. Sahu, U. Krupp, H.J. Christ, Fatigue crack initiation behavior in embrittled austenitic–ferritic stainless steel, Int. J. Fatigue 45 (2012) 8–14.
[10] K. Yamaguchi, K. Kanazawa, Influence of grain size on the low-cycle fatigue lives of austenitic stainless steels at high temperatures, Metall. Trans. A 11 (1980) 1691–1699.
[11] S. Xu, X.Q. Wu, E.H. Han, W. Ke, Y. Katada, Crack initiation mechanisms for low cycle fatigue of type 316Ti stainless steel in high temperature water, Mater. Sci. Eng. A 490 (2008) 16–25.
[12] X. Wu, E. Han, W. Ke, Y. Katada, Effects of loading factors on environmental fatigue behavior of low-alloy pressure vessel steels in simulated BWR water, Nucl. Eng. Des. 237 (2007) 1452–1459.
[13] H.P. Seifert, S. Ritter, H.J. Leber, Corrosion fatigue crack growth behaviour of austenitic stainless steels under light water reactor conditions, Corros. Sci. 55 (2012) 61–75.

[14] M. Kamaya, Environmental effect on fatigue strength of stainless steel in PWR primary water – role of crack growth acceleration in fatigue life reduction, Int. J. Fatigue 55 (2013) 102–111.
[15] R. Ebara, Corrosion fatigue crack initiation behavior of stainless steels, Procedia Eng. 2 (2010) 1297–1306.
[16] K.M. Perkins, M.R. Bache, Corrosion fatigue of a 12%Cr low pressure turbine blade steel in simulated service environments, Int. J. Fatigue 27 (2005) 1499–1508.
[17] Y. Yi, B. Lee, S. Kim, J. Jang, Corrosion and corrosion fatigue behaviors of 9Cr steel in a supercritical water condition, Mater. Sci. Eng. A 429 (2006) 161–168.
[18] M.F. Chiang, M.C. Young, J.Y. Huang, Effects of hydrogen water chemistry on corrosion fatigue behavior of cold-worked 304L stainless steel in simulated BWR coolant environments, J. Nucl. Mater. 411 (2011) 83–89.
[19] H. Cho, B.K. Kim, I.S. Kim, C. Jang, Low cycle fatigue behaviors of type 316LN austenitic stainless steel in 310°C deaerated water–fatigue life and dislocation structure development, Mater. Sci. Eng. A 476 (2008) 248–256.
[20] H. Sun, X. Wu, E. Han, Y. Wei, Effects of pH and dissolved oxygen on electrochemical behavior and oxide films of 304SS in borated and lithiated high temperature water, Corros. Sci. 59 (2012) 334–342.
[21] H. Sun, X. Wu, E. Han, Effects of temperature on the oxide film properties of 304 stainless steel in high temperature lithium borate buffer solution, Corros. Sci. 51 (2009) 2840–2847.
[22] J. Xu, X. Wu, E. Han, The evolution of electrochemical behaviour and oxide film properties of 304 stainless steel in high temperature aqueous environment, Electrochim. Acta 71 (2012) 219–226.
[23] W. Kuang, X. Wu, E. Han, The oxidation behaviour of 304 stainless steel in oxygenated high temperature water, Corros. Sci. 52 (2010) 4081–4087.
[24] M. Fulger, M. Mihalache, D. Ohai, S. Fulger, S.C. Valeca, Analyses of oxide films grown on AISI 304L stainless steel and Incoloy 800HT exposed to supercritical water environment, J. Nucl. Mater. 415 (2011) 147–157.
[25] M.F. Montemor, M.G.S. Ferreira, N.E. Hakiki, M. Da Cunha Belo, Chemical composition and electronic structure of the oxide films formed on 316L stainless steel and nickel based alloys in high temperature aqueous environments, Corros. Sci. 42 (2000) 1635–1650.
[26] X. Cheng, Z. Feng, C. Li, C. Dong, X. Li, Investigation of oxide film formation on 316L stainless steel in high-temperature aqueous environments, Electrochim. Acta 56 (2011) 5860–5865.
[27] D.A. Shirley, High-resolution X-ray photoemission spectrum of the valence bands of gold, Phys. Rev. B 5 (1972) 4709–4714.
[28] J.F. Moulder, F.S. William, E.S. Peter, Handbook of X-ray and Ultraviolet Photoelectron Spectroscopy, Perkin-Elmer Corporation, Eden Prairie, MN, 1992.
[29] K. Obrtlık, J. Polák, M. Hájek, A. Vašek, Short fatigue crack behaviour in 316L stainless steel, Int. J. Fatigue 19 (1997) 471–475.
[30] M. Kamaya, M. Kawakubo, Strain-based modeling of fatigue crack growth – an experimental approach for stainless steel, Int. J. Fatigue 44 (2012) 131–140.
[31] A. El Bartali, V. Aubin, S. Degallaix, Fatigue damage analysis in a duplex stainless steel by digital image correlation technique, Fatigue Fract. Eng. M. 31 (2008) 137–151.
[32] J.Y. Huang, M.C. Young, S.L. Jeng, J.J. Yeh, J.S. Huang, R.C. Kuo, Corrosion fatigue behavior of low alloy steels under simulated BWR coolant conditions, J. Nucl. Mater. 405 (2010) 17–27.
[33] Z. Zhang, H. Zhao, H. Zhang, Z. Yu, J. Hu, L. He, J. Li, Effect of isothermal aging on the pitting corrosion resistance of UNS S82441 duplex stainless steel based on electrochemical detection, Corros. Sci. 93 (2015) 120–125.
[34] M. Gholami, M. Hoseinpoor, M.H. Moayed, A statistical study on the effect of annealing temperature on pitting corrosion resistance of 2205 duplex stainless steel, Corros. Sci. 94 (2015) 156–164.
[35] T. Magnin, C. Ramade, J. Lepinoux, L.P. Kubin, Low-cycle fatigue damage mechanisms of F.c.c. and B.c.c. polycrystals: homologous behaviour, Mater. Sci. Eng. A 118 (1989) 41–51.
[36] Y.Q. Wang, J. Han, B. Yang, X.T. Wang, Strengthening of σ phase in a $Fe_{20}Cr_9Ni$ cast austenite stainless steel, Mater. Charact. 84 (2013) 120–125.
[37] T. Kruml, J. Polák, K. Obrtlík, S. Degallaix, Dislocation structures in the bands of localised cyclic plastic strain in austenitic 316L and austenitic–ferritic duplex stainless steels, Acta Mater 45 (1997) 5145–5151.
[38] J. Man, T. Vystavěl, A. Weidner, I. Kuběna, M. Petrenec, T. Kruml, J. Polák, Study of cyclic strain localization and fatigue crack initiation using FIB technique, Int. J. Fatigue 39 (2012) 44–53.
[39] I. Alvarez-Armas, U. Krupp, M. Balbi, S. Hereñú, M.C. Marinelli, H. Knobbe, Growth of short cracks during low and high cycle fatigue in a duplex stainless steel, Int. J. Fatigue 41 (2012) 95–100.
[40] M.C. Marinelli, U. Krupp, M. Kübbeler, S. Hereñú, I. Alvarez-Armas, The effect of the embrittlement on the fatigue limit and crack propagation in a duplex stainless steel during high cycle fatigue, Eng. Fract. Mech. 110 (2013) 421–429.